Research Article

Dissociation of hydrazine on tetrahedral Ni_4 cluster by density functional theory

Ghanashyam Roy[1] · **Asoke P. Chattopadhyay**[2]

Abstract
Sequential dissociation of hydrazine has been studied on Ni_4 cluster applying density functional theory (DFT) methods. Two routes of dissociation have been discussed. The first path (A) is the consecutive dissociation of four N–H bonds to form surface N_2 via intermediate product diimide, N_2H_2. The second path (B) is the dissociation of N–N bond to form two NH_2 species leading to formation of surface ammonia. The second elementary steps for both the routes show the highest activation energy barrier; for example in path A, $N_2H_3 + H \rightarrow N_2H_2 + 2H$, E_{Act} is 1.19 eV and in path B, $2NH_2 \rightarrow NH + H + NH_2$, E_{Act} is 1.71 eV. These are the rate-determining steps. NBO analysis shows that adsorption of hydrazine and ammonia is due to strong delocalisation of the lone pairs to the higher energy states of the cluster. Adsorption and dissociation of hydrazine and ammonia are thermodynamically feasible at standard conditions. Formation of N_2 is a slow exothermic process, whereas N–N bond dissociation to form two NH_2 species is a faster and highly exothermic process. NH species binds by two Ni–N covalent bonds. N species binds the cluster by three Ni–N bonds and three strong lone pair delocalisation at three-fold site. Removal of these intermediates needs higher energy of activation. Thus, the formation and dehydrogenation of ammonia are slow and lengthy processes. New catalysts could be designed in such a way that N–N bond might not be dissociated, which is happening due to absence of lone pair of N1(LP) to Rydberg orbital of N2(RY*) delocalisation or vice versa.

Keywords Hydrazine · Ammonia · Adsorption · Dissociation · Ni_4 · DFT

1 Introduction

Nowadays, fuel cells are considered as non-conventional and renewable source of energy, but the commercial application of fuel cells is limited due to higher price and lower availability of platinum electro-catalysts, which are used for their excellent catalytic property and high resistance in acidic medium. Recently, the demand for cheaper metallic electro-catalysts, viz. nickel, cobalt or alloys, e.g. Ni–Co, Ni–Fe, etc. [1–3]., and hydrazine-based fuel cells, viz. anion exchange membrane (AEM), direct hydrazine fuel cell (DHFC), room-temperature hydrazine–air direct-liquid fuel cells (DLFC) [4–6], have made them promising candidates for their excellent performance, lower cost, higher conductivity and longevity.

Hydrazine is C-free hydrogen-rich (15.5 wt%) high power density fuel, available in liquid form at room temperature, which can be used as an alternative source of hydrogen instead of hydrogen itself. Hydrazine-based fuel cells can be used in vehicles due to higher cell potential, e.g. + 1.56 V in air–hydrazine cell. The cell reaction takes place in 40–80 °C and produces higher power density than hydrogen fuel cell (5400 W h L^{-1}) [7]. In alkaline medium, the anodic cell reaction for hydrazine is

Electronic supplementary material The online version of this article (https://doi.org/10.1007/s42452-019-0392-9) contains supplementary material, which is available to authorized users.

✉ Ghanashyam Roy, ghanashyamroy96@gmail.com | [1]Department of Chemistry, Krishnagar Government College, Krishnagar, West Bengal 741101, India. [2]Department of Chemistry, University of Kalyani, Kalyani, West Bengal 741235, India.

SN Applied Sciences (2019) 1:377 | https://doi.org/10.1007/s42452-019-0392-9

Received: 15 December 2018 / Accepted: 21 March 2019 / Published online: 29 March 2019

$N_2H_4 + 4OH^- \rightarrow N_2 + 4H_2O + 4e^-$. To understand the cell reaction mechanism, several studies have proposed that electro-oxidation of hydrazine on noble metal catalysts takes place through catalytic breaking of N–H bonds, which cannot be identified experimentally due to fast electro-oxidation of the surface hydrogen [8, 9]. But the mechanism of non-faradic or electron-less decomposition reactions, $N_2H_4 \rightarrow N_2 + 2H_2$ (complete dissociation) and $3N_2H_4 \rightarrow N_2 + 4NH_3$ (incomplete dissociation) are also important, which depend upon the catalyst and reaction conditions [10–16].

Many investigations have been carried out throughout the decades to understand the mechanism of adsorption and dissociation of hydrazine on transition metal surfaces both experimentally and theoretically. Some earlier DFT investigations reported that both gauche and trans-hydrazine preferentially adsorbed on top site, whereas cis isomer liked to adsorb on bridging site of Pt(111) [17] and Ni(111) [18] surfaces. Also, trans- or anti-conformer was found to be the most stable geometry vis-a-vis cis and gauche isomers on these surfaces. However, experimentally, Alberas et al. [19] identified by XPS that both the N atoms are adsorbed on the same site on Pt(111) surface and N–N bond is parallel to the surface, suggesting retention of N–N bond and favouring dissociation of N–H bond. Till now, full understanding of bonding nature of hydrazine with Ni catalyst is not clear. Huang et al. [20] identified NH_3, N_2H_2, H_2 and N_2 species on Ni(100) surface experimentally on a temperature-programmed reaction spectroscopy (TPRS) at 90 K and pressure at 7.4×10^{-11} Tor.

Several mechanisms for the dissociation of hydrazine have been proposed. Sequential dehydrogenation of hydrazine with the formation of adsorbed N_2H_3, N_2H_2, N_2H and N_2 species on metal surfaces is shown in several studies [19, 21, 22]. In contrast, some authors [16, 21, 23, 24] reported N–N bond breaking taking place to form two NH_2 species which lead to the formation of N, N_2, H_2 and NH_3, and proposed that formation of ammonia can slow down cell efficiency [25–27]. Zhang et al. [28] studied adsorption and dissociation of NH_3 on Ni_{13}, $Ni_{12}Cu$ and Cu_{13} clusters and observed that the processes are exothermic. But why formation of ammonia reduces the cell efficiency is yet to be understood.

Although pure hydrazine is toxic, hydrated hydrazine ($N_2H_4{\cdot}H_2O$) is less toxic and considered as a potential source of hydrogen (8 wt%). However, it deactivates pure nickel metal due to the formation of surface N as nitride. On the other hand, Ni-based bimetallic catalysts, such as Ni–Pt, Ni–Ir and Ni–Rh, etc., can perform 100% selective H_2 conversion at moderate conditions [29–42]. Although several catalysts have been designed for 100% selective dehydrogenation, which route is favourable for hydrogen generation—H–N bond dissociation pathway or N–N bond dissociation pathway—remains unclear. Yin et al. [43] generated hydrogen from hydrazine monohydrate with 52% selectivity applying nickel nanoparticles on carbon support and proposed theoretically that both N–H and N–N bond breaking pathways operate to form N_2 and NH_3, respectively, on Ni(111) surface at different surface coverages. Presently, the demand for cheap nanomaterial-based fuel cells is increasing, and to understand the reaction mechanism on nanoparticles, study of adsorption and dissociation of fuel molecules on small clusters is important [44]. In recent decades, application of nickel clusters or nanoparticles from diatomic to bulk has evoked wide interest both experimentally and theoretically due to their better catalytic and optical properties, high conductivity and lower cost than other noble metals [45–50]. For example, Xu et al. [51] experimentally obtained 100% conversion of hydrous hydrazine to hydrogen applying Rh–Ni nanoparticles of Rh/Ni ratio 4:1. Oliaee et al. [52] proved that octahedral Pt–Ni/C nanocatalysts having greater stability, durability and selectively can convert hydrazine to H_2.

Recently, small cluster-based theoretical studies are very important to understand the mechanism of surface reactions at molecular level. For example, Pelegrini et al. [53] studied the dissociation of hydrazine on tetrahedral Pt_4 cluster via $NHNH_3$ and N_2H_5 intermediates as a model to understand the reactivity of hydrazine on surface of platinum nanocluster-based electrodes. Gordon et al. [54] reported hydrazine dissociation applying tetrahedral Ir_4 and prismatic Ir_6 clusters supported on small alumina slabs, e.g. Al_6O_9, Al_8O_{15}, $Al_{10}O_{16}$, etc. as a model of Shell 405 catalyst. However, several small Ni_4 cluster-based calculations are also reported to clarify the decomposition of small molecules on such surfaces [55–57]. To our knowledge, the dissociation of hydrazine on Ni_4 cluster has not been reported till date.

Adsorption and dissociation of hydrazine on Ni_4 cluster have been studied in the present work applying density function theoretic (DFT) methods. This is justified by earlier theoretical and experimental results. Two pathways of dissociation have been introduced. The complete mechanism of sequential dissociation of hydrazine may involve elementary steps which are represented and discussed at molecular level applying ab initio molecular orbital theory and natural bond order (NBO) analysis. Formation and dissociation of the intermediate product NH_3 are also discussed with corresponding energy values.

2 Computational methods

Geometry optimisations were performed at the generalised gradient approximation (GGA) [58] using Perdew–Burke–Ernzerhof (PBE) [59, 60] exchange correlation

functional in Gaussian 09W package [61]. Geometry optimisations were confirmed by the number of imaginary frequency values to be zero. For Ni atom, the Los Alamos National Laboratory basis set of double-ζ quality (LANL2DZ) [62] was used, and the corresponding scalar relativistic effective core potential replaced the inner-shell electrons. 6-311+G(3*df*,2*p*) [63] basis set is used for N and H atoms. During optimisation, all the atoms were relaxed.

The three-dimensional tetrahedral Ni_4 cluster is used as a model to understand the reactivity of hydrazine at molecular level on surface of Ni catalyst particle. The optimised geometrical parameters of Ni_4 cluster is presented in our earlier papers [56, 57]. However, to obtain stable configuration of adsorption, different possible adsorption configurations were optimised by placing the conformers of hydrazine on the binding sites of Ni_4 cluster, as shown in Fig. 1b. Pelegrini et al. [53] used LANL2DZ basis set in B3LYP [64, 65], MO6 [66, 67] and PBE [59, 60] functionals for tetrahedral Pt_4 cluster. Reina et al. [68] applied LANL2DZ/M06 level of theory for small clusters of Cu, Ag and Au.

Calibration of the method is done comparing experimental methods applying different functional and basis sets (Table 1). Results using PBE functional are nearer to the experimental data. For example, N–H and N–N bond lengths for isolated hydrazine are 1.024–1.029 Å (1.021 [72]), 1.438 Å (1.449 Å [72]), and for Ni_2 is 2.123 Å [57] (2.15 Å [71]) as reported in our earlier paper.

The binding or adsorption energy (E_b) of N_2H_4 on the cluster is calculated from Eq. (1).

$$E_b = E_{Ni_4/N_2H_4} - \left(E_{Ni_4} + E_{N_2H_4}\right) \quad (1)$$

where E_{Ni_4/N_2H_4}, E_{Ni_4} and $E_{N_2H_4}$ are electronic energies for adsorption configuration, bare cluster and isolated N_2H_4, respectively. The dissociation energy (E_{diss}) and other thermodynamic energies for dissociation are calculated

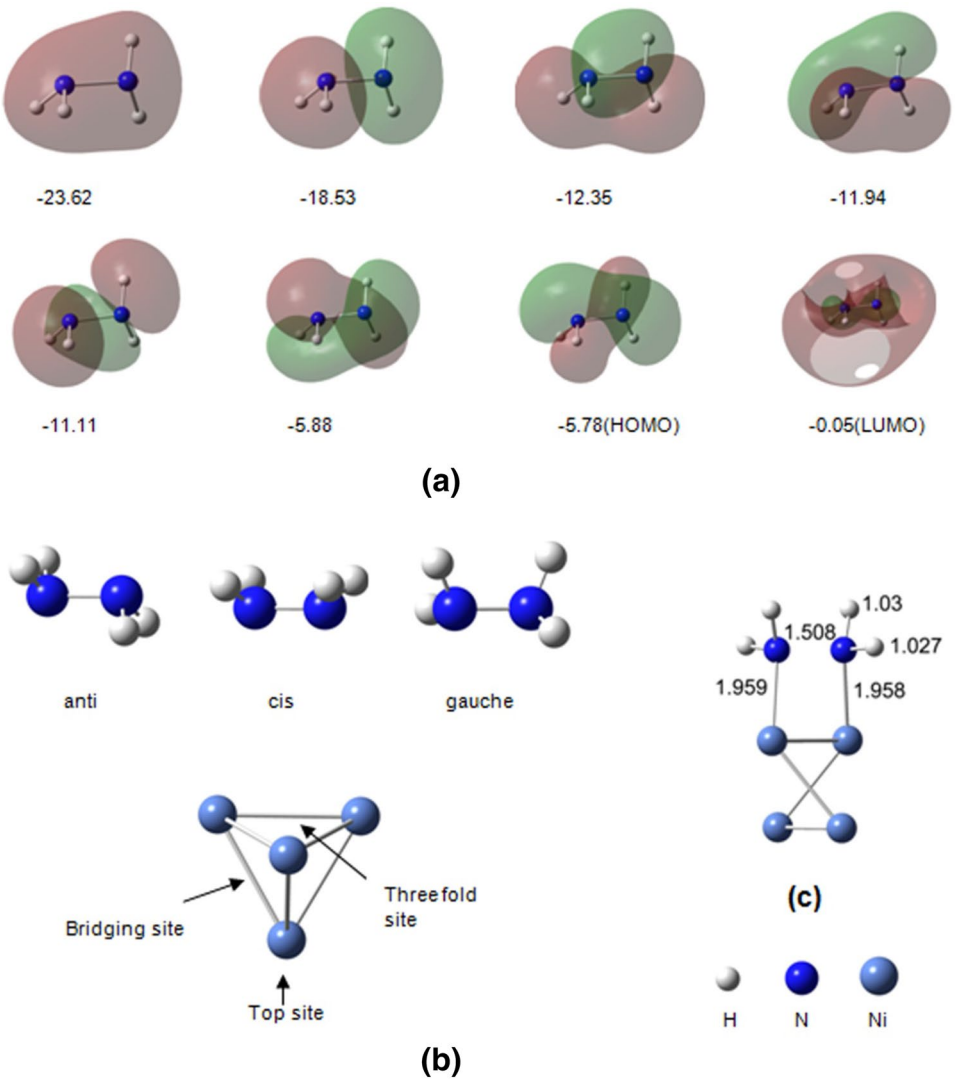

Fig. 1 **a** MOs of hydrazine, energies (in eV), **b** anti, cis and gauche isomers and tetrahedral Ni_4 cluster, **c** Adsorbed hydrazine on Ni_4 cluster. H = Hydrogen, N = Nitrogen, Ni = Nickel

Table 1 Calculated Ni–Ni bond distances of Ni_2 and Ni_4, and N–H and N–N bond distances of N_2H_4

DFT methods	Ni_2	Ni_4		N_2H_4	
	Ni–Ni	Ni–Ni	Point group	N–H	N–N
B3LYP	2.091	2.148	D_{2d}	1.011, 1.014	1.432
M06	2.075	2.252	D_{2d}	1.011, 1.014	1.415
PBE	2.123[f]	2.322[f]	D_{2d}	1.020, 1.024	1.438
Ref.	2.08[b]	2.30[a]		1.02, 1.03[d]	1.437[d]
Exp.	2.15[c]			1.021[e]	1.449[e]

[a]Ref. [69], [b]Ref. [70], [c]Ref. [71], [d]Ref. [18], [e]Ref. [72], [f]Ref. [57]

as the difference between the energies of dissociated state ($E_{DS/G/H}$) and energies for adsorption system ($E_{Ads/G/H}$),

$$E_{Diss/\Delta G/\Delta H} = E_{DS/G/H} - E_{Ads/G/H} \quad (2)$$

The synchronous transit-guided quasi-Newton (STQN) [73] method was used to determine transition state (TS) geometry which is verified by the presence of a single imaginary frequency. Transition states (TS) were correlated with the initial states (IS) and dissociation states (DS) by intrinsic reaction coordinate (IRC) plot. The electronic energy barrier for each step is calculated from Eq. (3).

$$E_{Act} = E_{TS} - E_{IS} \quad (3)$$

where E_{TS} and E_{IS} are energies of the transition state and initial state, respectively. NBO analysis describes accurate natural Lewis structures with the most possible electron density orbital to describe intra- or intermolecular interactions between filled orbitals (e.g. 2-centre bonding (BD) and lone pair (LP)) and virtual orbitals (e.g. antibonding (BD*), unoccupied 1-centre orbital (LP*) and Rydberg orbital (RY*)). The second-order Fock matrix analysis provides the donor–acceptor interaction energies, which are calculated as Eq. (4),

$$E_2 = \Delta E_{ij} = q_i \frac{F(i,j)^2}{\varepsilon_j - \varepsilon_i} \quad (4)$$

where q_i occupancy of the donor, ε_i and ε_j are diagonal elements and $F(i, j)$ is the off-diagonal element. All the molecular geometries and orbitals are shown in GaussView package [74].

3 Results

3.1 Adsorption of N_2H_4 on Ni_4 cluster

The optimised adsorption geometry and calculated energies on Ni_4 cluster are presented in Fig. 1c and Table 2, respectively. The calculated Gibbs free energy and heat of reaction are negative indicating adsorption is a thermodynamically feasible and exothermic reaction at normal conditions. Since both the N atoms are chemically equivalent, the two Ni atoms are bonded cis fashion at bridging site on Ni_4 cluster forming a rectangular geometry. Ni–N bond distances are 1.959 and 1.958 Å. The structure of adsorbed hydrazine is distorted gauche conformer, where N–H and N–N bond distances are elongated to (1.027 Å, 1.03 Å) and 1.508 Å, respectively. The calculated adsorption or binding

Table 2 Adsorption energy (E_{Ads}, eV), reaction energy (E_{Diss}, eV), Gibbs free energy (ΔG, eV), activation energy barrier (E_{Act}, eV), Δq[a] (charge transfer, e) and single imaginary frequency (ν_i, cm^{-1}) at standard temperature and pressure

Reactions on cluster	Step	E_{Ads}/E_{Diss}	ΔH	ΔG	E_{Act}	Δq	ν_i
Adsorption		−1.56	−1.51	−2.12		−0.17	
Dissociation							
Path A							
$N_2H_4 \rightarrow N_2H_3 + H$	1	−0.61	−0.74	−0.72	0.43	0.28	−1003.8
$H + N_2H_3 \rightarrow N_2H_2 + 2H$	2	−0.64	−0.92	−0.91	1.19	0.48	−1183.38
$N_2H_2 + 2H \rightarrow N_2H + 3H$	3	−1.35	−1.81	−1.79	0.42	0.73	−1101.15
$N_2H + 3H \rightarrow N_2 + 4H$	4	−2.16	−2.74	−2.72	0.71	0.62	−528.92
Path B							
$N_2H_4 \rightarrow NH_2 + NH_2$	1	−2.78	−2.85	−2.83	0.02	0.65	−384.08
$NH_2 + NH_2 \rightarrow NH_2 + NH + H$	2	−1.09	−1.30	−1.30	1.71	1.02	−886.92
$NH_2 + NH + H \rightarrow NH_3 + NH$	3	−0.68	−0.54	−0.64	0.56	0.44	−961.06
NH_3 adsorption		−1.30	−1.20	−1.92		−0.13	
NH_3 dissociation	1	−0.30	−0.46	−0.35	0.38	0.60	−207.82
	2	−0.29	−0.65	−0.52	0.96	0.96	−68.48
	3	−0.70	−1.17	−1.00	0.35	1.07	−741.90
N_2 formation	4	−0.18	−0.20	−0.12	1.05	0.34	−349.28

[a]Δq = Net charge of the cluster atoms after adsorption or dissociation (q_2) − charge of the isolated cluster (q_1)

energies of hydrazine are – 1.56 eV on Ni_4 cluster, – 1.28 eV on Pt_4 cluster [53] and – 1.86 eV on Ir_6/alumina [54], but 0.52–0.80 eV on bridging position of Ni (111) surface [18], indicating that clusters bind hydrazine more strongly than surfaces which can favour dissociation. For example, corner atoms of Shell 405 nanoparticles can decompose hydrazine more efficiently than bulk Ir (111) surface [28].

The Kohn–Sham MOs of the Ni_4 cluster are shown in an earlier study [57], and MOs of isolated gauche hydrazine are presented in Fig. 1a. The MOs of the adsorption interaction are shown in Fig. 2. There are seven MOs from – 22.75 to – 11.46 eV, where valence electrons (VEs) of hydrazine delocalise, and from – 10.83 to – 5.52 eV, VEs of Ni_4 cluster delocalise to the virtual MOs of hydrazine.

From NBO analysis, it appears that for isolated N_2H_4 molecule, the two N–H bond (BD) pairs are slightly different. One pair is upward to the N atoms' plane for the gauche isomer (Fig. 1b), and occupancy and hybrid nature of N for upward N–H bond pair are 1.99571 ($sp^{2.95}$, 74.46% *p*). For the opposite bond pair, the corresponding values

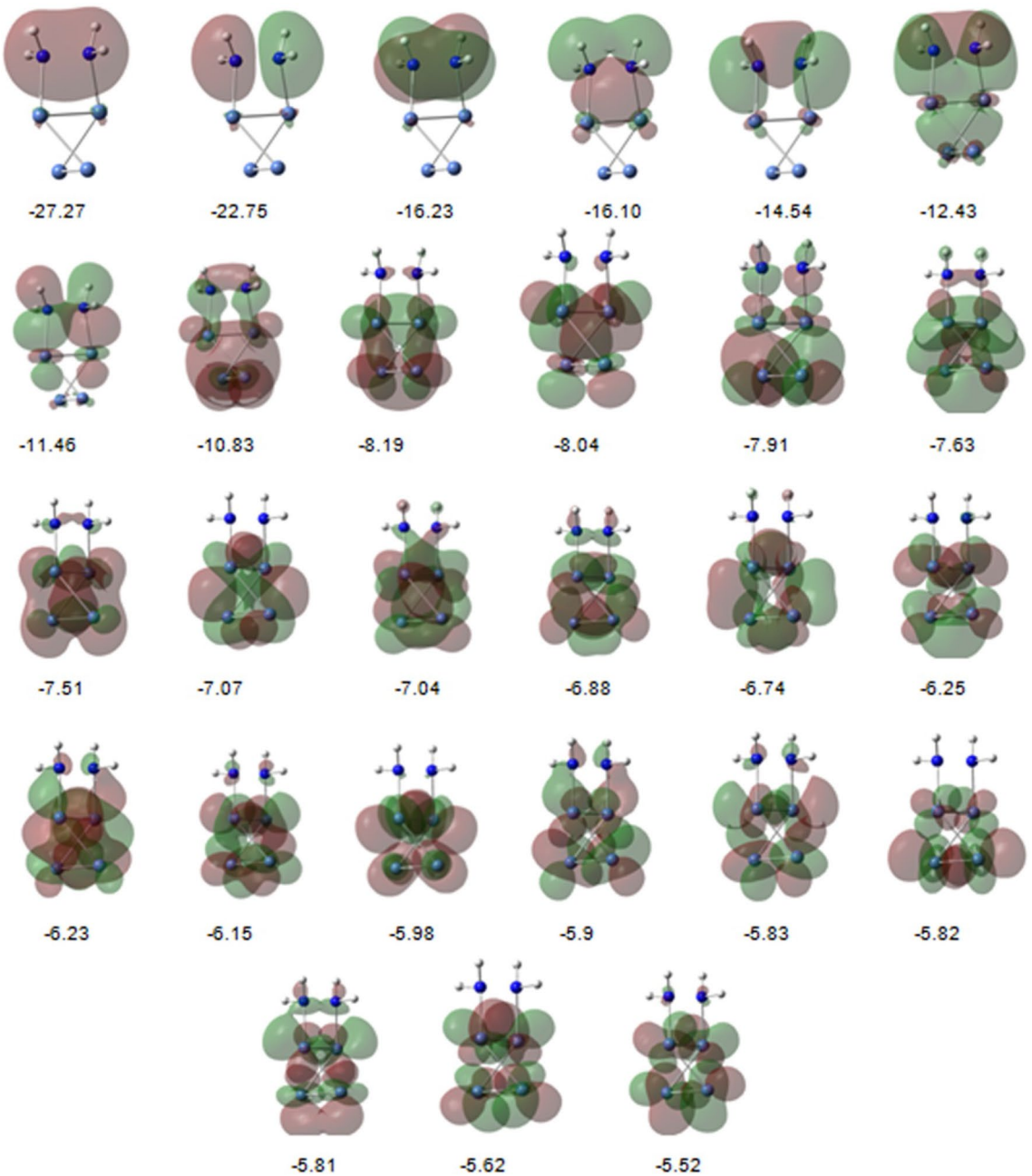

Fig. 2 Kohn-Sham MOs of hydrazine adsorption on Ni_4 cluster and energies (in eV)

are 1.99287 ($sp^{2.94}$, 74.45% *p*), respectively. For N–N bond, occupancy is 1.99813, hybridisation of both N atoms being ($sp^{2.86}$, 73.85% *p*). The two lone pairs N(LP) have the same occupancy 1.97097 and hybridisation ($sp^{3.2}$, 75.97% *p*). From natural population analysis during adsorption, charge transfer to the cluster is − 0.17 eV, indicating dissociation of N_2H_4 is favourable at standard conditions. This result is similar to what was found in an earlier study [75]. NBO analysis for adsorption system (Fig. 1c) suggests that occupancies are 1.98970 for the upward N–H bond pair and 1.98102 for the opposite N–H bond pair. Hybridisation of the two entities is ($sp^{2.81}$, 73.68% *p*) and ($sp^{2.64}$, 72.47% *p*), respectively. For N–N bond, the occupancy is 1.99562 and the hybridisation of N being ($sp^{3.51}$, 77.54% *p*). Two lone pairs N (LP) have occupancies 1.83205 and 1.83178 and have the same hybridisation ($sp^{3.14}$, 75.81% *p*). Thus, the occupancy of the lone pair N(LP) of hydrazine decreases (-0.13 e) during adsorption, due to delocalisation of the lone pairs to the higher energy states of the cluster, indicating major charge transfer takes place from the lone pair orbital.

The second-order Fock matrix analysis is presented in Table S1 of Supporting Information. The lone pair of each N atom is found to delocalise to empty valence orbital of Ni_4 cluster, e.g. N1(LP) → Ni1(LP)* and N2(LP) → Ni2(LP)*. The delocalisation energies (DE) are 15.07 and 15.10 kcal/mol, respectively. Again, lone pairs of the cluster delocalise to Rydberg orbitals of N. The delocalisation energies (DE) for Ni1(LP) → N(RY)* and Ni2(LP) → N(RY)* are 4.18 and 4.08 kcal/mol, respectively. Thus, hydrazine is adsorbed to Ni_4 cluster by strong delocalisation energy of the lone pairs of N atoms, although no bond formation is observed between them at the adsorption state. The N–H and N–N bonds delocalise to the vacant LP* orbitals of the clusters at 3.54 kcal/mol and 4.70 kcal/mol, respectively, indicating weakening of the bonds, making dissociation favourable on the Ni_4 cluster. The lone pair of both N (LP) atoms delocalise to Rydberg orbital of H (RY)*. The delocalisation energy of N1(LP) → H1(RY*) is 0.74 kcal/mol which increases N–H bond strength, but N1(LP) → N2(RY*) or N2(LP) → N1(RY*) delocalisations are diminished during adsorption. However, for isolated hydrazine, delocalisation energies for N1(LP) → H1(RY*) and N1(LP) → N2(RY*) are 0.63 kcal/mol and 1.30 kcal/mol, respectively, indicating that during adsorption N–N bond becomes weaker. Thus, the cleavage of N–N bond is easier than N–H bond due to adsorption.

3.2 Dissociation of N_2H_4 on Ni_4 cluster

The two pathways of dehydrogenation of hydrazine on Ni_4 cluster are discussed, and their energies and potential energy surfaces are presented in Table 2 and Fig. 4, respectively. The adsorption geometry of hydrazine on Ni_4 cluster (in Fig. 1c) is considered as the initial state 1 (IS1) for both path A and path B.

Path A Dissociation geometries are presented in Fig. 3a. Four sequential elementary steps of N–H bond dissociation are discussed. In step 1, $N_2H_4 \rightarrow N_2H_3 + H$, where the dissociation of N1–H1 bond on adjacent b_2 site elongates to 1.397 Å at transition state (TS1) and 2.977 Å at dissociated state (DS1), forming N_2H_3 species by bond Ni1–N1(1.874 Å) on the cluster. The activation barrier for this step is 0.43 eV, whereas the value is 0.71 eV on Ni (111) [43] for gauche isomer. In step 2, dissociation of second N2–H2 bond leads to the formation of diimide; the elementary step is: $N_2H_3 + H \rightarrow N_2H_2 + 2H$. The dissociation of N2–H2 bond takes place on adjacent b_2 site which elongates to 1.416 Å and 3.047 Å at TS2 and DS2, respectively, forming diimide (N_2H_2) as shown in DS2, Fig. 3a. The calculated activation barrier is 1.19 eV, and on Ni(111) surface, the value is 0.85 eV [43].

In step 3, the elementary step is: $N_2H_2 + 2H \rightarrow N_2H + 3H$. Dissociation of N1–H3 bond takes place, which is elongated to 1.331 Å and 3.014 Å at TS3 and DS3, respectively, forming N_2H species. It binds through Ni1–N1 bond, and double bond character arises at TS3. The calculated activation barrier is 0.42 eV. On Ni(111) surface; however, the process is exothermic by − 0.26 eV and the activation barrier is 0.91 eV [43]. For step 4, $N_2H + 3H \rightarrow N_2 + 4H$, dissociation of N2 – H4 bond takes place, which is elongated to 1.11 Å and 2.544 Å at TS4 and DS4, respectively. This step is the most exothermic, with ΔH of − 2.74 eV and dissociation barrier of 0.71 eV. This is similar to Ni(111) surface study, where the process is exothermic by -0.93 eV, having a moderate barrier of 0.80 eV [43]. The N–N bond distance gradually decreases from 1.508 Å (adsorption state), 1.469 Å (DS1), 1.354 Å (DS2), 1.258 Å (DS3) to 1.164 Å (DS4) during dissociation of N–H bonds. These values follow the same order with Ni(111) surface study [43]. Therefore, Ni_4 cluster can efficiently bind and decompose hydrazine as bulk Ni(111) surface.

The adsorbed N_2 binds at a cis pattern, N–Ni bond distances being 1.917 and 1.812 Å. The elementary step 2 is the rate-determining step which shows the highest activation energy barrier of 1.19 eV, as both Ni1–N1 and N2–H2 bonds break simultaneously.

The NBO analysis for dissociation in path A is given in Table S1, Supporting Information. At dissociation state 1 (DS1), N_2H_3 species binds to the cluster with Ni1–N1 σ-bond, with occupancy of 1.86865 (27% Ni +73% N). The hybridisation of Ni1 is ($sp^{0.18}d^{1.93}$, 62.02% *d*) and of N1 is ($sp^{11.18}$, 91.51% *p*). The occupancy of N1–H3, N2–H2 and N2–H4 bonds is 1.97228, 1.98354, 1.98179, respectively. Hybridisation of N atoms is ($sp^{3.50}$, 77.47% *p*) ($sp^{2.92}$,

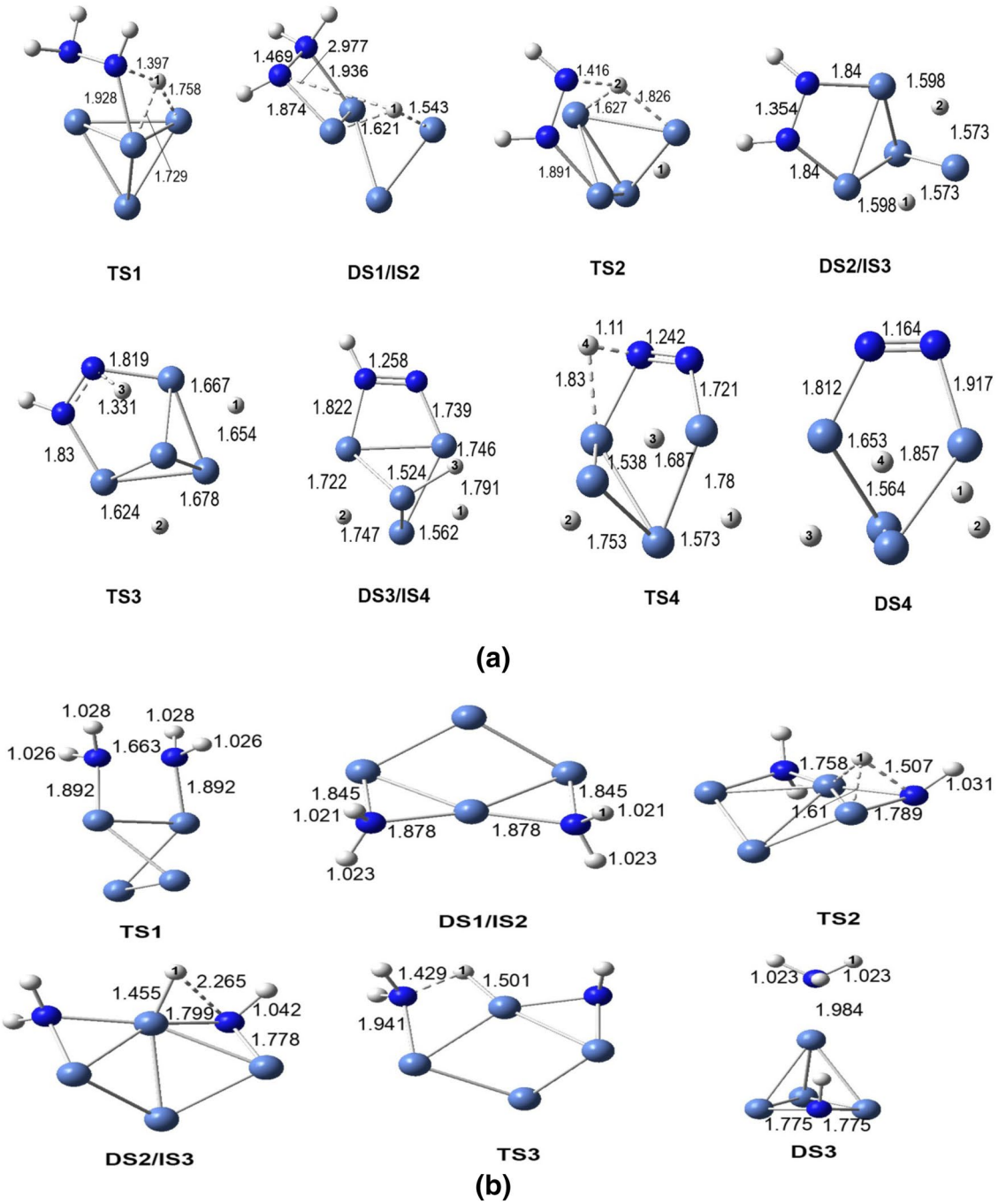

Fig. 3 **a** Dissociation geometries of path A, N_2 formation, **b** dissociation geometries of path B, NH_3 formation. TS1 (transition state 1), DS1/IS2 (dissociation state 1 is considered as Initial state 2 for step 2), TS2 (transition state 2), DS2/IS3 (dissociation state 2 is considered as initial state 3 for step 3), TS3 (transition state 3), DS3/IS4 (dissociation state 3 is considered as initial state 4 for step 4), TS4 (transition state 4) and DS4 (dissociation state 4)

74.46% *p*) and ($sp^{3.17}$, 75.98% *p*), respectively. For N1–N2 bond, occupancy is 1.99461. Hybridisation of N1 is ($sp^{4.58}$, 81.75% *p*) and of N2 is ($sp^{2.92}$, 74.46% *p*). The occupancy and hybridisation for LP of N1 are 1.87252 and ($sp^{0.92}$, 47.91% *p*), respectively. The values for N2 are 1.72635 and ($sp^{2.98}$, 74.88% *p*), respectively. At dissociation step 2 (DS2), N_2H_2 species binds on the cluster by two diagonal σ-bonds. The Ni2–N1 bond has occupancy of 1.85438 (67% Ni + 33% N), with hybridisation of N1 $sp^{73.22}$ (98.54% *p*). The Ni1–N2 bond has occupancy of 1.85358 (67% Ni + 33% N), with hybridisation of N2 $sp^{73.23}$ (98.54% *p*). In dissociation state 3 (DS3), N_2H binds with Ni1–N1 bond, with

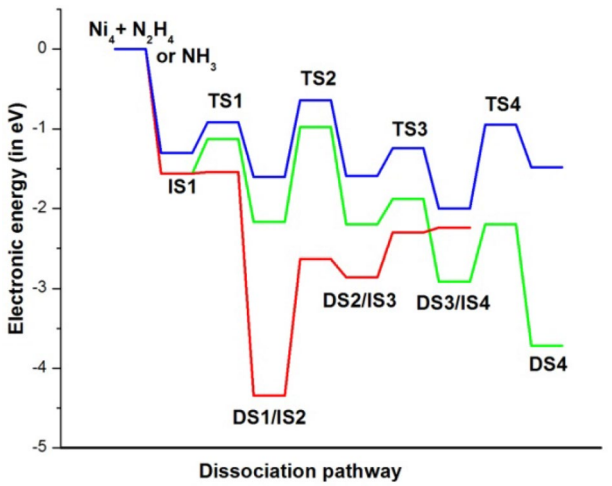

Fig. 4 Potential energy diagram of the reaction paths. Green line represents formation of N_2 via N_2H_2 intermediate (Path A). Red line shows formation of NH_3 (path B). Blue line represents NH_3 dissociation and N_2 formation

occupancy 1.96995 (58% Ni + 42% N). Here, hybridisation of Ni1 is ($sp^{2.57}d^{99.99}$, 99.67% *d*) and of N1 is ($sp^{23.19}$, 95.44% *p*). Again, a N1–N2 σ-bond forms with occupancy 1.99535, hybridisation of N1 being ($sp^{2.48}$, 70.92% *p*) and of N2 being ($sp^{1.92}$, 65.67% *p*). Similarly, formation of a N1–N2 π-bond occurs, with occupancy 1.97075, and hybridisation $sp^{99.99}$ for both N atoms (99.60% *p*). For dissociation state 4 of N_2 (surface), a N1–N2 σ-bond forms, with occupancy 1.99634. Hybridisation of N1 is ($sp^{1.78}$, 63.77% *p*) and of N2 is ($sp^{1.68}$, 62.53% *p*). The two π-bonds have occupancy and hybridisation of 1.98143 ($sp^{99.99}$, 99.64% *p*) and 1.89708 ($sp^{99.99}$, 99.98% *p*) for both N atoms. Occupancy for the lone pair of N1(LP) is 1.83504, with hybridisation ($sp^{0.56}$, 35.84% *p*). For N2(LP), the corresponding values are 1.81529 and ($sp^{0.59}$, 37.23% *p*). Thus, after four sequential N–H bonds in dissociation of hydrazine, π-character of bond orbital (BD) increases and s character of the lone pair (LP) of N atoms increases. In steps 2 and 4, dissociation of two bonds, e.g. (N2–H2, Ni1–N1) and (N2–H4, Ni1–N1), takes place simultaneously. This causes higher activation energy for both the steps. But step 4 requires less dissociation energy barrier than step 2 due to change of hybrid nature of the Ni1–N1 σ-bond, i.e. *p* character of N1 ($sp^{11.18}$, 91.51% *p*) for N_2H_3 species and ($sp^{23.19}$, 95.44% *p*) for N_2H species.

Ab initio MOs for the dissociation steps DS1–DS4 are presented in Figure S1-S4, Supporting Information. N_2 molecule binds at bridging site by σ-type overlap of ($s + dz^2$) at -14.64 eV, with few π donor and acceptor interactions, indicating N_2 is strongly bound to the cluster.

Path B Dissociation geometries are presented in Fig. 3b. In step 1, $N_2H_4 \rightarrow NH_2 + NH_2$, the adsorbed hydrazine is dissociated to two NH_2 species binding on two adjacent bridging sites. N – N bond distance is extended to 1.663 Å at TS1 and 3.642 Å at DS1. In step 2, $NH_2 + NH_2 \rightarrow NH_2 + NH + H$, dissociation of NH_2 to NH and H takes place. The dissociated NH bond is elongated to 1.507 Å and 2.265 Å at TS2 and DS2, respectively. In step 3, $NH_2 + NH + H \rightarrow NH_3 + NH$, the adsorbed H is transferred to nearest NH_2 species to form NH_3 molecule. The new N–H bond forming distances at TS3 and DS3 are 1.429 Å and 1.029 Å, respectively. However, step 2 or dissociation of NH_2 species is the rate-determining step, with calculated activation barrier of 1.71 eV. Yin et al. [43] calculated N–N bond dissociation barriers as 0.49, 0.36, 1.08 eV for anti, cis and gauche isomer, respectively, on Ni(111) surface. All these values were exothermic. Since both the N atoms are bonded to the surface for the cis isomer, N–N bond length is increased to 1.485 Å and favours dissociation. However, N–N distance was observed as more stretched on Ni_4 cluster, the value being 1.508 Å. Dissociation barrier for gauche isomer which adsorbed in cis fashion is 0.02 eV. But the formation of ammonia can be slow due to the higher dissociation energy barrier for step 2 in path B.

The NBO analysis for path B is given in Table S2, Supporting Information. At DS1, two NH2 species are co-adsorbed. Occupancies of two pairs of N–H bonds are 1.98405 (N1–H1, N2–H4) and 1.98925 (N1–H3, N2–H2). Hybridisations of N1 are ($sp^{2.76}$, 73.32% *p*) and of N2 is ($sp^{2.51}$, 71.44% *p*). Two pairs of LP on N1 have occupancies 1.69589, 1.60794 and hybridisation of LP1 ($sp^{36.86}$, 97.34% *p*) and LP2 ($sp^{1.37}$, 57.52% *p*), respectively. Another two pairs of LP on N2 have occupancies 1.69578, 1.60796 and hybridisations of LP1 as (sp^{37}, 97.34% *p*) and of LP2 as ($sp^{1.37}$, 57.70% *p*), respectively. Therefore, more number of lone pairs can slow down the N–H bond dissociation due to repulsive nature of the electrons. In DS2, NH_2 species binds by Ni2–N1 bond, with occupancy 1.90511 (22% Ni + 78% N). The hybridisations are: Ni2 ($sp^{0.87}d^{1.59}$, 46% *d*) and N1 ($sp^{2.72}$, 73.06% *p*). NH species forms Ni2–N2 and Ni3–N2 bonds, with occupancies 1.78902 (35%Ni + 65%N) and 1.84171 (32%Ni + 68%N), respectively. The hybridisations are: Ni2 ($sp^{2.8}d^{4.99}$, 57% *d*), N2 ($sp^{10.42}$, 90.84% *p*), Ni3 ($sp^{0.1}d^{1.54}$, 60% *d*), N2 ($sp^{8.10}$, 88.54% *p*), respectively. The lone pair of N1 (LP) has occupancy 1.65751 and hybridisation ($sp^{3.90}$, 79.55% *p*). Corresponding one of N2 (LP) has occupancy 1.84402 and hybridisation ($sp^{0.70}$, 41.14% *p*). At DS3, NH_3 (adsorbed) has three N–H bond of occupancies 1.99229 (N1–H1), 1.99256 (N1–H2) and 1.99256 (N1–H3). The hybridisations of N are ($sp^{2.69}$, 72.81% *p*; $sp^{2.70}$, 72.90% *p*; $sp^{2.70}$, 72.90% *p*), respectively. The LP of N1 has occupancy 1.84459 and hybridisation ($sp^{4.32}$, 81.20% *p*). Moreover, NH species binds with Ni2–N2 of occupancy 1.90377 and hybridisation of N is ($sp^{10.52}$, 91.13% *p*). For N2–H4 bond, occupancy is 1.78543 and hybridisation of

N2 is ($sp^{41.22}$, 97.38% *p*). LP of N2 has occupancy 1.83962 and hybridisation ($sp^{0.52}$, 34.01% *p*).

Both NH_2 species get co-adsorbed (DS1) to the cluster by strong delocalisation of two lone pairs of each N atom. This is shown as N1(LP1) → Ni1(LP*)/Ni2(LP*). The energy values are 12.32 and 41.45 kcal/mol, respectively. In co-adsorption of NH_2 and NH species (DS2), delocalisation energy of N1(LP) of NH_2 species is 40.09 kcal/mol. Corresponding value for N2(LP) of NH species is 23.39 kcal/mol. At DS3, lone pairs of NH_3 and NH species (DS3) bind to the cluster by 21.16 and 17.90 kcal/mol, respectively. Thus, NH species strongly binds to the cluster forming two Ni–N bonds with strong delocalisation energy. These are highly stable on the cluster. Huang et al. [20] observed the formation of diimide (N_2H_2) on Ni(100) surface from 200-450 K and proposed that the formation occurs due to recombination of two NH species. But, Yin et al. [43] proposed that diimide formation takes place via $N_2H_4 \rightarrow NH_2 + NH_2 \rightarrow NH + NH \rightarrow N_2H_2$ which is energetically unfavourable process, with E_{Act} 1.32 eV.

Thus, there will be a competition between two routes of dissociation and production of hydrogen will be lower. Similar results are obtained on Ni(111) surface by Yin et al. [43]. It was proved experimentally that 52% H_2 selectivity takes place over nickel nanoparticles supported on carbon from 50 to 60 °C, with rate of the reaction around 10–20 h^{-1}. Therefore, the values computed with the Ni_4 cluster in the present case compare favourably with previous calculations and experimental results. The Ni_4 cluster is thus a plausible model to study reactivity of hydrazine on Ni nanoparticles.

3.3 Adsorption and dissociation of NH_3

To understand the fate of ammonia formed during hydrazine decomposition, the adsorption and dissociation geometries of NH_3 on Ni_4 cluster were considered, as shown in Fig. 6. It has been observed that both adsorption and dissociation are thermodynamically favourable processes. The energy values are represented in Table 2. The occupied MOs of NH_3 act as a donor from − 22.71 (weak), − 12.84 (strong) and − 12.81 eV (strong), whereas one strong acceptor overlap occurs at -9.24 eV, as shown in Fig. 5. From NBO analysis, NH_3 appears at isolated state, with three N–H bonds, having occupancy 1.99932, hybridisation of N being ($sp^{2.98}$, 74.79% *p*). There is also a lone pair N (LP) with occupancy 1.99554 and hybridisation ($sp^{2.98}$, 74.77% *p*). For adsorption state, the three N–H bonds have occupancy (1.99091), with hybridisation of N as ($sp^{2.62}$, 72.34% *p*). But occupancy of the lone pair N (LP) greatly decreases to 1.83833 with hybridisation ($sp^{4.62}$, 82.20% *p*). However, from the second-order Fock matrix analysis, as presented in Table S3 (Supporting Information), the lone pair of the N atom delocalises to higher energy states of Ni1, e.g. N1(LP) → Ni1(LP)*. The delocalisation energy (DE) for the step is 22.34 kcal/mol and for Ni(LP) → N(RY), DE 4.46 kcal/mol, indicating N of ammonia is a strong donor and a weak Rydberg acceptor. Moreover, the lone pair delocalisation energy for N(LP) → H(RY*) decreases from 1.48 kcal/mol (for free NH_3 molecule) to 1 kcal/mol, indicating weakening of N–H bond.

The calculated adsorption energy is -1.30 eV, same as that on Ni_{13} cluster [27]. The formation of NH_2 is the rate-determining step. Dissociation of ammonia is a three-step process: $NH_3 \rightarrow NH_2 + H \rightarrow NH + 2H \rightarrow N + 3H$. Adsorption of ammonia is the initial state 1 (IS1) for the dissociation process, as shown in Fig. 6. However, second step (DS2) or dissociation of NH_2 species is the rate-determining step, with E_{act} of 0.96 eV. The potential energy plot is represented as blue line in Fig. 4.

However, after complete dissociation of ammonia, resulting surface N formed as nitride, observed as tridentate ligand in threefold site of the Ni_4 cluster. The MOs are shown in Figure S5 (Supplementary Information). The nitride can reduce activity of the Ni catalyst. Thus, Plana et al. [76] reported that 100% conversion of ammonia requires high temperature at 880 K applying Ni catalyst supported on alumina-coated cordierite monoliths.

Moreover, formation of N_2 is a thermodynamically feasible process, but the activation energy barrier is quite high at 1 eV. The co-adsorption of two N atoms is considered as the initial step for N_2 formation. Thus, although the dehydrogenation of ammonia thermodynamically feasible process, nevertheless, the formation of ammonia from hydrazine and dehydrogenation of it is a lengthy process due to more number of higher activation energy barriers.

NBO analysis for NH_3 dissociation (in Figure S3, Supporting Information) provides the following information. At dissociation state 1 (DS1), NH_2 species binds forming Ni1–N1 bond, with occupancy 1.90894 (29%Ni + 71%N). The hybridisation of Ni1 is ($sp^{0.12}d^{1.13}$, 50% *d*) and of N1 is ($sp^{3.02}$, 75.07% *p*). The two N–H bonds have occupancies 1.99192 and 1.98686, and hybridisations of N as ($sp^{2.59}$, 72.11% *p*; $sp^{2.66}$, 72.64% *p*), respectively. The lone pair N(LP) is of occupancy 1.76781 and hybridisation $sp^{4.0}$ (79.96% *p*). At DS2, NH species binds with Ni1–N1 bond, with occupancy 1.96452 (50% Ni + 50% N). Hybridisation of Ni1 is ($sp^{0.95}d^{74.54}$, 97.45% *d*) and of N is ($sp^{1.86}$, 50.41% *p*). The N–H bond has occupancy 1.96532 and hybridisation ($sp^{2.16}$, 68.27% *p*). The two N(LP)s are of occupancy 1.72169 and 1.51578, with hybridisations ($sp^{1.99}$, 66.55% *p*) and (s^0p^1, 99.94% *p*), respectively. For DS3, N species binds to the cluster with three Ni–N σ-bonds, having similar occupancy 1.99024 (57%Ni + 43%N) and hybridisation of Ni ($sp^{0.45}$ $d^{99.99}$,

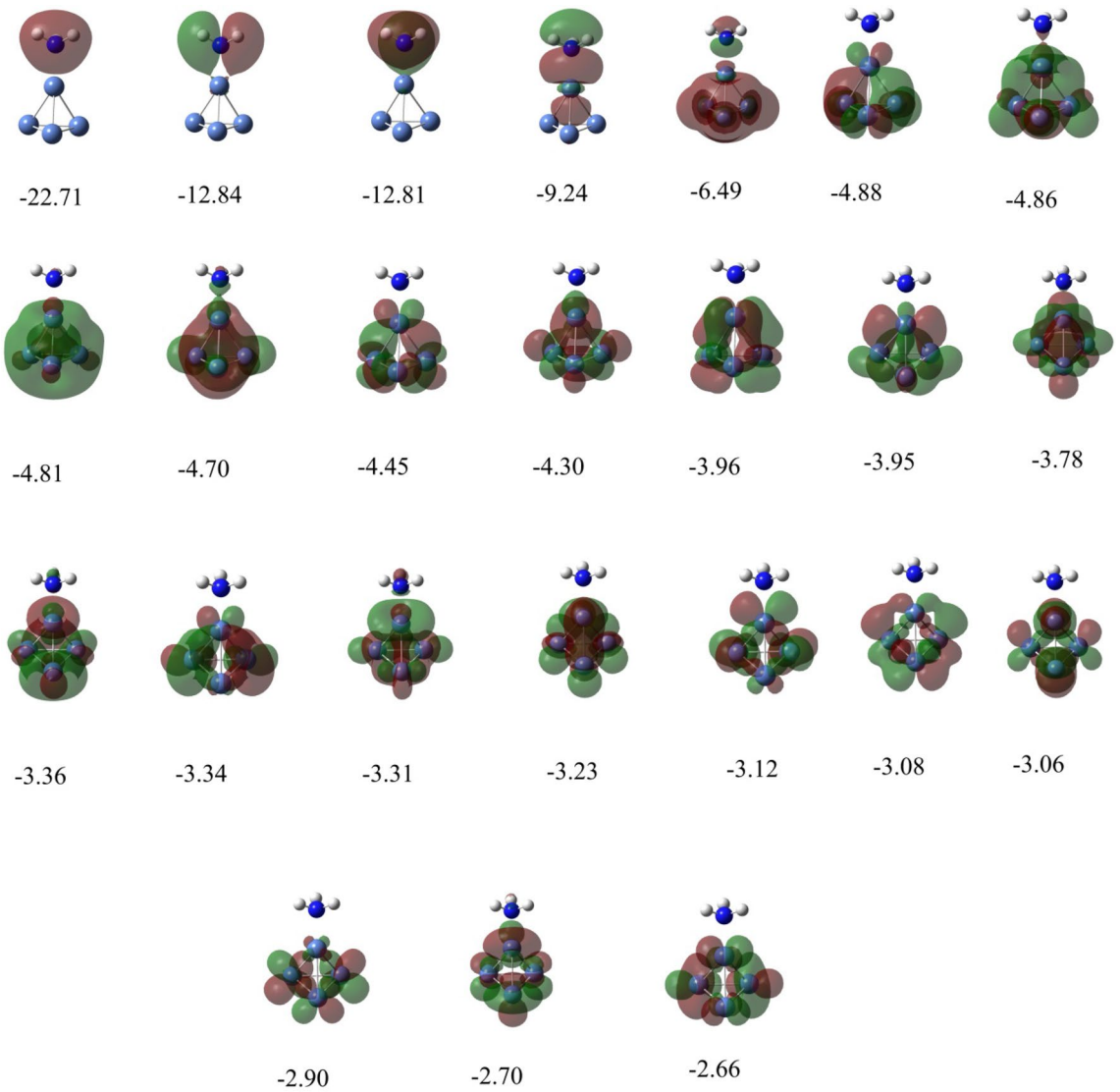

Fig. 5 NH_3 adsorption MOS on Ni_4 cluster and energies (in eV)

99.22% *d*) and of N ($sp^{24.70}$, 95.58% *p*). A lone pair (LP) is also formed, with occupancy 1.76486 and hybridisation ($sp^{0.12}$, 10.95% *p*). Thus, N species binds to the surface by three Ni–N bonds, indicating higher heat of dissociation will be required to remove the N_2 gas from the surface of the catalyst.

The lone pair of each N atom for NH_2, NH and N delocalises to higher energy states of Ni_4, N(LP) → Ni(LP*). The delocalisation energy for NH_2 is 35.03 kcal/mol; for NH species two lone pairs, delocalisation energy values are (28.19, 29.95 kcal/mol) and (19.67, 22.03 kcal/mol). For N species, three delocalisation energies are identical at 24.02 kcal/mol.

4 Conclusion

1. Adsorption and dissociation of hydrazine and ammonia on Ni catalyst are simulated on a Ni_4 cluster as a finite surface prototype model for Ni catalyst, using density functional theory. Hydrazine binds to Ni_4 cluster by cis fashion coordinating two Ni atoms, and NH_3 binds at the top site of the Ni_4 cluster. Adsorption of both the molecules is due to strong delocalisation of the lone pair of nitrogen to higher energy states of the cluster. The delocalisation energy (DE) values are 15.07

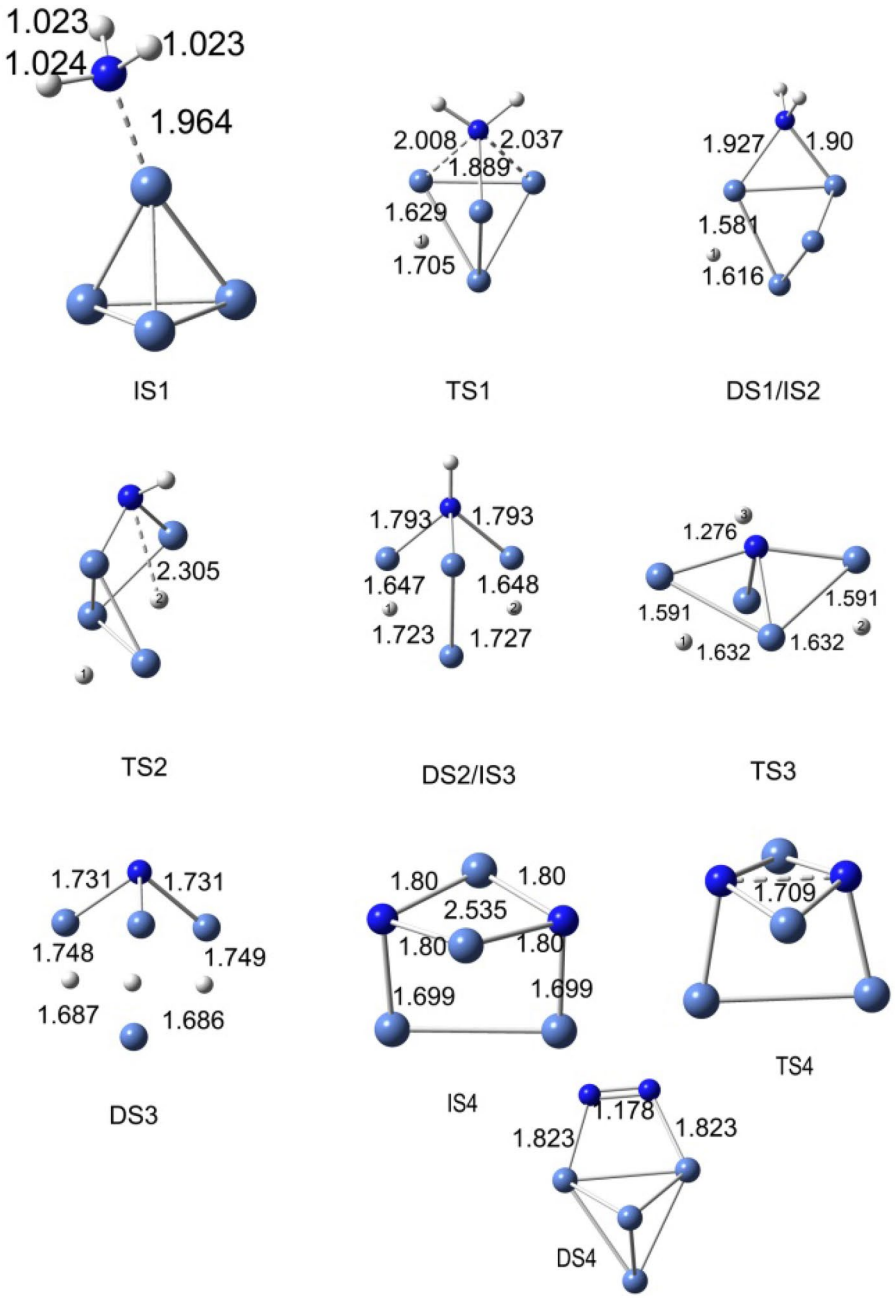

Fig. 6 Dissociation pathway of NH_3 and formation of N_2.IS1 (initial state 1), TS1 (transition state 1), DS1/IS2 (dissociation state 1, considered as initial state 2), TS2 (transition state 2), DS2/IS3 (dissociation state 2, considered as initial state 3), TS3 (transition state 3), DS3 (dissociation state 3), IS4 (initial state 4, co-adsorption of two N species), TS4 (transition state 4) and DS4 (dissociation state 4)

and 15.10 kcal/mol for hydrazine and 22.34 kcal/nol for ammonia.

2. The N–N bond distance of hydrazine increases from 1.438 to 1.508 Å due to absence of delocalisation of the lone pair N1(LP) → N2(RY*) or N2(LP) → N1(RY*) during adsorption. Dissociation of N–N bond is easier than of N–H bond due to strong donor–acceptor interaction via LP of two N and Ni_4 clusters and absence of delocalisation of N1(LP) → N2(RY*) or vice versa during adsorption. For free hydrazine, the DE value is 1.30 kcal/mol.
3. In path A, steps 2 and 4 show higher activation energy barriers at 1.19 eV and 0.71 eV due to dissociation of N–H and Ni–N bonds. Step 2 is the rate-determining step. Ni–N bond at DS1 or IS2 is *spd* hybrid, whereas for DS3 or IS4, it has mostly *pd* character. In path B, step 2 or dissociation of a NH_2 species, $2NH_2 \rightarrow NH + H + NH_2$, is the rate-determining step, with activation barrier of 1.71 eV. This is due to repulsive nature of two NH_2 species having two lone pairs present on each N atom.
4. All the processes are thermodynamically feasible. Formation of N_2 is a highly exothermic process, with

ΔH – 2.74 eV. Dehydrogenation of hydrazine through path A is easier than through path B, because the species formed throughout the process are N_2H_3, N_2H_2 and N_2H and finally N_2. Each N_2H_3 or N_2H species binds to the cluster by one Ni–N bond. N_2H_2 species binds to the cluster by two diagonal Ni–N weak bonds. Therefore, dissociation of these intermediates is easier. Finally, surface N_2 binds to the cluster by lone pair delocalisation, with DE values as 45 and 55 kcal/mol. No Ni–N bond formation has been observed, and removal of N_2 will be easier.

In path B, co-adsorption of two NH_2 species and two lone pairs on each N atom is repulsive in nature causing higher N–H bond dissociation energy barrier. Although ammonia formation needs higher activation barrier, NH formed in the final step binds the cluster by two Ni–N bonds. Therefore, removal or dissociation of the NH species may require higher energy barrier.

5. Thus, N–N bond rupture can slow down the cell performance due to formation of not only ammonia as a lengthy process of dehydrogenation but also formation of surface N as tridentate ligand which strongly binds at the three-fold site of the cluster. N species binds to the cluster by three Ni–N bonds. This investigation can be a clue for the future design of a perfect dehydrogenation catalyst for hydrazine.

Acknowledgements The authors gratefully acknowledge infrastructural support from DST-FIST and UGC-SAP grants to the Department of Chemistry, KU, and from DST-PURSE grant to the Faculty of Science, KU, for this research work.

Compliance with ethical standards

Conflict of interest On behalf of all authors, the corresponding author states that there is no conflict of interest.

References

1. Asazawa K, Sakamoto T, Yamaguchi S, Yamada K, Fujikawa H, Tanaka H, Oguro K (2009) Study of anode catalysts and fuel concentration on direct hydrazine alkaline anion exchange membrane fuel cells. Electrochem Soc 4(156):B509–B512
2. Wlodarczyk PP, Wlodarczyk B (2015) Ni-Co alloy as catalyst for fuel electrode of hydrazine fuel cell. China USA Bus Rev 5(14):269–279
3. Yang H, Zhong X, Dong Z, Wang J, Jin J, Ma J (2012) A highly active hydrazine fuel cell catalyst consisting of a Ni-Fe nanoparticle alloy plated on carbon materials by pulse reversal. RSC Adv (Commun) 2:5038–5040
4. Andrew MR, Gressler WJ, Johnson JK, Short RT, Williams KR (1972) Ionic conductivity of oxides based on Li_4SiO_4. J Appl Electrochem 2:327
5. Granot E, Filanovsky B, Presman I, Kuras I, Patolsky F (2012) Hydrazine/air direct-liquid fuel cell based on nanostructured copper anodes. J Power Sources 204:116–121
6. Yamada K, Asazawa K, Yasuda K, Ioroi T, Tanaka H, Miyazaki Y, Kobayashi T (2003) Investigation of PEM type direct hydrazine fuel cell. J Power Sources 115:236–242
7. Chinchilla JS, Asazawa K, Sakamoto T, Yamada K, Tanaka H, Strasser P (2011) Noble metal-free hydrazine fuel cell catalysts: EPOC effect in competing chemical and electrochemical reaction pathways. J Am Chem Soc 133:5425–5431
8. Fukumoto Y, Matsunaga T, Hayashi T (1981) Electrocatalytic activities of metal electrodes in anodic oxidation of hydrazine in alkaline solution. Electrochim Acta 26:631–636
9. Kodera T, Honda M, Kita H (1985) Electrochemical behavior on platinum in alkaline solution. Electrochim Acta 30:669
10. Gu H, Ran R, Zhou W, Shao Z, Jin W, Xu N, Ahn J (2008) Solid-oxide fuel cell operated on in situ catalytic decomposition products of liquid hydrazine. J Power Sources 177:323–329
11. Cho SJ, Lee J, Lee YS, Kim DP (2006) Characterization of Iridium catalyst for decomposition of hydrazine hydrate for hydrogen generation. Catal Lett 109:181–187
12. Zheng M, Cheng R, Chen X, Li N, Li L, Wang X, Zhang T (2005) A novel approach for CO-free H_2 production via catalytic decomposition of hydrazine. Int J Hydrogen Energy 30:1081–1089
13. Chen X, Zhang T, Zheng M, Wu Z, Wu W, Li C (2004) The reaction route and active site of catalytic decomposition of hydrazine over molybdenum nitride catalyst. J Catal 224:473–478
14. Armstrong WE, Ryland LB, Voge HH (1978) Catalyst comprising Ir or Ir and Ru hydrazine decomposition. US Patent 4:124–538
15. Santos JBO, Valenca GP, Rodrigues JAJ (2002) Catalytic decomposition of hydrazine on Tungsten carbide: the influence of adsorbed oxygen. J Catal 210:1–6
16. Prasad J, Gland JL (1991) Hydrazine decomposition on a clean rhodium surface: a temperature programmed reaction spectroscopy study. Langmuir 7:722–726
17. Agusta MK, Dino WA, David M, Nakanishi H, Kasai H (2011) Theoretical study of hydrazine adsorption on Pt (111): anti or cis? Surf Sci 605:1347–1353
18. Agusta MK, Kasai H (2012) First principles investigation of hydrazine adsorption conformations on Ni (111) surface. Surf Sci 606:766–771
19. Alberas DJ, Kiss J, Liu ZM, White JM (1992) Surface chemistry of hydrazine on Pt (111). Surf Sci 278:51–61
20. Huang XS, Rufael TS, Gland JL (1993) Diimide formation on the Ni(111) surface. Surf Sci 290:L673–L676
21. Wagner ML, Schmidt LD (1991) Adsorption and decomposition of H_2NCHO, D_2NCHO, N_2H_4, and NH_3 on Rh (111). Surf Sci Lett 257:A565
22. Maurel R, Menezo JC (1978) Catalytic decomposition of ^{15}N-labeled hydrazine on alumina-supported metals. J Catal 51:293–295
23. Johnson DW, Roberts MW (1980) Adsorption of hydrazine and ammonia on alumina. J Electron Spectrosc Relat Phenom 19:185–195
24. Grunze M (1979) The interaction of hydrazine with an Fe(111) surface. Surf Sci 81:603–625
25. Jiang HL, Singh SK, Yan JM, Zhang XB, Xu Q (2010) Liquid-phase chemical hydrogen storage: catalytic hydrogen generation under ambient conditions. Chemsuschem 3:541–549
26. Zhu QL, Xu Q (2015) Liquid organic and inorganic chemical hydrides for high-capacity hydrogen storage. Energy Environ Sci 8:478–512
27. Singh SK, Xu Q (2013) Nanocatalysts for hydrogen generation from hydrazine. Catal Sci Technol 3:1889–1900
28. Zhang PX, Wang YG, Huang YQ, Zhang T, Wu GS, Li J (2011) Density functional theory investigations on the catalytic

mechanisms of hydrazine decomposition on Ir(111). Catal Today 165:80–88
29. Singh SK, Xu Q (2010) Bimetallic Ni-Pt nanocatalysts for selective decomposition of hydrazine in aqueous solution to hydrogen at room temperature for chemical hydrogen storage. Inorg Chem 49:6148–6152
30. Singh SK, Xu Q (2010) Bimetallic nickel-iridium nanocatalysts for hydrogen generation by decomposition of hydrous hydrazine. Chem Commun 46:6545–6547
31. Singh AK, Yadav M, Aranishi K, Xu Q (2012) Temperature-induced selective enhancement in hydrogen generation from Rh-Ni nanoparticle-catalyzed decomposition of hydrous hydrazine. Int J Hydrogen Energy 37:18915–18919
32. He L, Huang Y, Wang A, Liu Y, Liu X, Chen X, Delgado JJ, Wang X, Zhang T (2013) Surface modification of Ni/Al_2O_3 with Pt: highly efficient catalysts for H_2 generation via selective decomposition of hydrous hydrazine. J Catal 298:1–9
33. Wang H-L, Yan J-M, Wang Z-LOS-I, Jiang Q (2013) Highly efficient hydrogen generation from hydrous hydrazine over amorphous $Ni_{0.9}Pt_{0.1}/Ce_2O_3$ nanocatalyst at room temperature. J Mater Chem A 1:14957–14962
34. Cao N, Yang L, Dai H, Liu T, Su J, Wu X, Luo W, Cheng G (2014) Immobilization of ultrafine bimetallic Ni-Pt nanoparticles inside the pores of metal-organic frameworks as efficient catalysts for dehydrogenation of alkaline solution of hydrazine. Inorg Chem 53:10122–10128
35. Cao N, Su J, Luo W, Cheng G (2014) Ni-Pt nanoparticles supported on MIL-101 as highly efficient catalysts for hydrogen generation from aqueous alkaline solution of hydrazine for chemical hydrogen storage. Int J Hydrogen Energy 39:9726–9734
36. Jiang Y, Kang Q, Zhang J, Dai H-B, Wang P (2015) High-performance nickel–platinum nanocatalyst supported on mesoporous alumina for hydrogen generation from hydrous hydrazine. J Power Sources 273:554–560
37. Zhong Y-J, Dai H-B, Jiang Y-Y, Chen D-M, Zhu M, Sun L-X, Wang P (2015) Highly efficient $Ni@Ni-Pt/La_2O_3$ catalyst for hydrogen generation from hydrous hydrazine decomposition: effect of Ni–Pt surface alloying. J Power Sources 300:294–300
38. Aika K, Ohhata T, Ozaki A (1970) Hydrogenolysis of hydrazine over metals. J Catal 19:140–143
39. Chen J, Yao Q, Zhu J, Chen X, Lu Z-H (2016) Rh-Ni nanoparticles immobilized on $Ce(OH)CO_3$ nanorods as highly efficient catalysts from hydrogen generation from alkaline solution of hydrazine. Int J Hydrogen Energy 41:3946–3954
40. Zhong D-C, Mao Y-L, Tan X, Zhong P, Liu L-X (2016) RhNi nanocatalyst: spontaneous alloying and high activity for hydrogen generation from hydrous hydrazine. Int J Hydrogen Energy 41:6362–6368
41. De S, Zhang J, Luque R, Yan N (2016) Ni-based bimetallic heterogeneous catalysts for energy and environmental applications. Energy Environ Sci 9:3314–3347
42. Dai H, Dai H-B, Zhong Y-J, Kang Q, Sun L-X, Wang P (2017) Kinetics of catalytic decomposition of hydrous hydrazine over CeO_2-supported Ni–Pt nanocatalysts. Int J Hydrogen Energy 42:5684–5693
43. Yin H, Qiu YP, Dai H, Gan LY, Dai HB, Wang P (2018) Understanding of selective H2 generation from hydrazine decomposition on Ni(111) surface. J Phys Chem C 122:5443–5451
44. Rodriguez-Kessler PL, Richard-Chavez JL (2015) Structures of FePt clusters and their interactions with O_2 molecule. Chem Phys Lett 622:34–41
45. Luo CL (2000) The structure of small nickel clusters: Ni_2–Ni_{19}. Model Simul Mater Sci Eng 8:95–101
46. Moskovits M, Hulse JE (1977) The ultraviolet-visible spectra of diatomic, triatomic, and higher nickel clusters. J Chem Phys 66:3988–3994
47. Nygren MA, Siegbahn PEM, Wahlgren U, Akeby H (1992) Theoretical ionization energies and geometries for nickel. J Phys Chem 96:3633–3640
48. Onal I, Sayar A, Uzun A, Ozkar SA (2009) Density functional study of Ni_2 and Ni_{13} nanoclusters. J Comput Theor Nanosci 6:867–872
49. Parks EK, Zhu L, Ho J, Riley SJ (1994) The structure of small nickel clusters. Ni_3–Ni_{15}. J Chem Phys 100:7206–7222
50. Singh SK, Singh AK, Aranishi K, Xu Q (2011) Noble-metal-free bimetallic nanoparticle-catalyzed selective hydrogen generation from hydrous hydrazine for chemical hydrogen storage. J Am Chem Soc 133:19638–19641
51. Singh SK, Xu Q (2009) Complete conversion of hydrous hydrazine at room temperature for chemical hydrogen storage. J Am Chem Soc 131:18032–18033
52. Oliaee SN, Zhang C, Hwang SY, Cheung HM, Peng Z (2016) Hydrogen production via hydrazine decomposition on model platinum-nickel nanocatalyst with a single (111) facet. J Phys Chem C 120:9764–9772
53. Pelegrini M, Parreira RLT, Ferrao LFA, Caramori GF, Ortolan AO, da Silva EH, Roberto-Neto O, Rocco JAFF, Machado FBC (2016) Hydrazine decomposition on small platinum cluster: the role of N_2H_5 intermediate. Theor Chem Acc 135:58
54. Schmidt MW, Gordon MS (2013) The decomposition of hydrazine in gas phase and over an iridium catalyst. Z Phys Chem 227:1301–1336
55. Wang Y, Su Y, Zhu M, Kang L (2015) Mechanism of CO methanation on Ni_4/γ-Al_2O_3 and Ni_3Fe/γ-Al_2O_3 catalyst: a density functional theory study. Int J Hydrogen Energy 40:8864–8876
56. Roy G, Chattopadhyay AP (2017) Dissociation of methane on Ni_4 cluster: a DFT study. Comput Theor Chem 1106:7–14
57. Roy G, Chattopadhyay AP (2018) Reactivity of CO on Ni_4 cluster-effect of spin multiplicity and H doping: a DFT investigation. Spectrochim Acta Part A Mol Biomol Spectrosc 204:362–369
58. White JA, Bird DM (1994) Implementation of gradient-corrected exchange-correlation potential in Car-Parrinello total-energy calculations. Phys Rev B 50:4954
59. Perdew JP, Burke K, Ernzerhof M (1996) Generalized gradient approximation made simple. Phys Rev Lett 77:3865
60. Perdew JP, Burke K, Ernzerhof M (1997) Generalized gradient approximation made simple. Phys Rev Lett 78:1396
61. Frisch, M J, Trucks GW, Schlegel HB, Scuseria GE, Robb MA, Cheeseman JR, Scalmani G, Barone V, Petersson GA, Nakatsuji H, Li X, Caricato M, Marenich A, Bloino J, Janesko BG, Gomperts R, Mennucci B, Hratchian HP, Ortiz JV, Izmaylov AF, Sonnenberg JL, Williams-Young D, Ding F, Lipparini FF, Egidi F, Goings J, Peng B, Petrone A, Henderson T, Ranasinghe D, Zakrzewski VG, Gao J, Rega N, Zheng G, Liang W, Hada M, Ehara M, Toyota K, Fukuda R, Hasegawa JM, Ishida J, Nakajima T, Honda Y, Kitao O, Nakai H, Vreven T, Throssell K, Montgomery JA, Peralta JA, Ogliaro F, Bearpark M, Heyd JJ, Brothers E, Kudin KN, Staroverov VN, Keith T, Kobayashi R, Normand J, Raghavachari K, Rendell A, Burant JC, Iyengar SS, Tomasi J, Cossi M, Millam JM, Klene M, Adamo C, Cammi R, Ochterski JW, Martin RL, Morokuma K, Farkas O, Foresman J B, Fox DJ. Gaussian 09, Revision A.02, Gaussian, Inc, Wallingford CT, 2016
62. Hay PJ, Wadt WR (1985) Ab initio effective core potential for molecular calculations. Potential for the transition metal atoms Sc to Hg. J Chem Phys 82:270
63. Chung-Phillips A, Jebber KA (1995) Ab initio studies of critical conformations in ethane, methylamine, methanol, hydrazine, hydroxyl amine, and hydrogen peroxide. J Chem Phys 102:7080
64. Becke AD (1993) Density functional thermochemistry. J Chem Phys 98:5648–5652
65. Lee C, Yang W, Parr RG (1988) Development of the Colle-Salvetti correlation-energy formula into a functional of the electron density. Phys Rev B 37:785–789

66. Zhao Y, Truhlar DG (2011) Applications and validations of the Minnesota density functionals. Chem Phys Lett 502:1–13
67. Zhao Y, Truhlar DG (2007) The M06 suite of density functionals for main group thermochemistry, thermochemical kinetics, noncovalent interactions, excited states, and transition elements: two new functionals and systematic testing of four M06-class functionals and 12 other functionals. Theor Chem Acc 120:215–241
68. Reina M, Martinez A (2018) Cu, Ag and Au clusters as air pollutants hunters. Comput Theor Chem 1130:15–23
69. Petkov PS, Vayssilov GN, Kruger S, Rosch N (2006) Structure, stability, electronic and magnetic properties of Ni_4 clusters containing impurity atoms. Phys Chem Chem Phys 8:1282–1291
70. Rodríguez-Kessler PL, Rodríguez-Domínguez AR (2015) Stability of Ni clusters and the adsorption of CH_4: first-principles calculations. J Phys Chem C 119:12378–12384
71. Pinegar JC, Langenberg JD, Arrington CA, Spain EM, Morse MD (1995) Ni_2 revisited: reassignment of the ground electronic state. J Chem Phys 102:666–674
72. Kohata K, Fukuyama T, Kuchitsu K (1982) Molecular structure of hydrazine as studied by gas electron diffraction. J Phys Chem 86:602
73. Peng C, Ayala PY, Schlegel HB, Frisch MJ (1996) Using redundant internal coordinates to optimize equilibrium geometries and transition state. J Comp Chem 17:49
74. Frisch A, Hratchian HP, Dennington II RD, Keith TA, Millam J, Nielsen AB, Holder AJ, Hiscocks J Gaussview Version 5.0, Gaussian, Inc., 340 Quinnipiac, Street, Building 40, Wallingford, CT 06492, USA (2009)
75. Roy G, Chattopadhyay AP (2018) Methane dissociation on bimetallic $AuNi_3$, Au_2Ni_2 and Au_3Ni clusters: a DFT study. Chem Select 3:3133–3140
76. Plana C, Armenise S, Monzon A, Garcıa-Bordeje E (2010) Ni on alumina-coated cordierite monoliths for in situ generation of CO-free H_2 from ammonia. J Catal 275:228–235